

# Thermal Fractionalization of Quantum Spins in a Kitaev Model

Joji Nasu,<sup>1</sup> Masafumi Udagawa,<sup>2</sup> and Yukitoshi Motome<sup>2</sup>

<sup>1</sup>*Department of Physics, Tokyo Institute of Technology, Ookayama, 2-12-1, Meguro, Tokyo 152-8551, Japan,*

<sup>2</sup>*Department of Applied Physics, University of Tokyo, Hongo, 7-3-1, Bunkyo, Tokyo 113-8656, Japan*

(Dated: December 25, 2018)

Thermodynamic properties of a Kitaev model defined on a honeycomb lattice are investigated from the viewpoint of fractionalization of quantum  $S = 1/2$  spins into two types of Majorana fermions, itinerant and localized. Performing a finite-temperature ( $T$ ) quantum Monte Carlo simulation, we find that the entropy of the system is released successively at two well-separated  $T$  scales, as a clear indication of the thermal fractionalization. We show that the high- $T$  crossover, which is driven by itinerant Majorana fermions, is closely related with the development of short-range spin correlations. On the other hand, the low- $T$  crossover originates in thermal fluctuations of fluxes composed of localized Majorana fermions, by which the spectrum of itinerant Majorana fermions is significantly disturbed. As a consequence, the specific heat shows apparently  $T$ -linear behavior in the fluctuating flux state with well-developed short-range spin correlations, although it should be  $T^2$  in the low- $T$  limit due to the Dirac semimetallic spectrum in the uniform flux sector. We also show that the flux fluctuations affect the gapless-gapped boundary. Our results indicate that the fractionalization is experimentally observable in the specific heat and spin correlations.

PACS numbers: 75.10.Kt, 75.70.Tj, 75.10.Jm

The fractionalization of electrons in solids into more fundamental degrees of freedom is one of the central topics in modern condensed matter physics. A prototypical example is found in one-dimensional strongly correlated electron systems: charge and spin degrees of freedom in an electron are separated and behave as independent particles termed holon and spinon [1]. In the insulating magnets with geometrical frustration, a different form of fractionalization is also anticipated to occur. For instance, the existence of the elementary excitation carrying a half of spin, named spinon, is predicted in a quantum spin liquid (QSL) [2], and emergence of magnetic monopoles is suggested in spin ice systems [3]. Another fractionalization was pointed out in heavy fermion systems as well. The half residual entropy in the two-channel impurity Kondo system is understood from the fractionalization of  $S = 1/2$  impurity spin into two Majorana fermions [4].

A quantum spin model, called the Kitaev model, has recently attracted considerable attention in broad areas of research, not only condensed matter physics but statistical physics and quantum information [5]. This model is composed of  $S = 1/2$  spins with bond-dependent interactions on a honeycomb lattice. Such peculiar interactions were suggested to be realized in the systems with strong spin-orbit coupling, such as iridium oxides [6]. The most striking feature of this model is that it is exactly solvable due to the existence of  $Z_2$  conserved quantity on each hexagon, termed flux. The ground state dictates both gapless and gapped QSL phases depending on the exchange coupling constants. The exact solution is provided by representing  $S = 1/2$  spins by two types of Majorana fermions: one is localized and composes the fluxes, and the other forms itinerant bands [7–9]. The latter itinerant Majorana fermions determine the excitation spectrum in the QSLs. Thus, the fractionalization of spins into Majorana fermions is not just a mathematical tool but physically important in the Kitaev model.

A natural question arising here is how high-temperature ( $T$ )

paramagnetic spins are fractionalized into Majorana fermions when cooling the system. In one-dimensional electron systems, the spin-charge separation plays a key role in explaining their thermodynamic properties, in particular, in comparison with experiments. The thermodynamic properties in the Kitaev model and its extensions have also been studied, mainly for explaining the magnetism in iridium oxides [10–15], but the fractionalization was not addressed in most of the previous studies. Among them, however, the authors pointed out the significance of fractionalization in a peculiar phase transition at finite  $T$  in a three-dimensional extension of the Kitaev model [13, 14]: the phase transition is governed by thermal excitations of localized Majorana fermions. Nevertheless, the relevance of fractionalization remains unclear, in particular, to the experimentally-observable quantities, such as the specific heat and spin-spin correlations. Considering the distinct roles of two species of Majorana fermions in the ground state, it is quite interesting to clarify how the fractionalization affects the finite- $T$  properties of QSLs.

In this Letter, we investigate the effect of fractionalization of quantum spins on the thermodynamics of the Kitaev model on a honeycomb lattice. By applying the unbiased quantum Monte Carlo (QMC) method, we show that the two Majorana fermions, itinerant and localized, release their entropy successively at two well-separated  $T$  scales. We elucidate that each crossover has an impact on experimental observables: the high- $T$  one, driven by itinerant Majorana fermions, corresponds to the development of spin correlations between neighboring sites, while the low- $T$  one originating from thermal fluctuations of localized Majorana fermions is accompanied by a sizable change in the excitation spectrum of itinerant Majorana fermions. This leads to apparent  $T$ -linear behavior of the specific heat in the intermediate  $T$  state with well-developed short-range spin correlations, though  $T^2$  behavior is anticipated for the Dirac semimetallic spectrum in the ground state. Moreover, we show that the thermal excita-

tion of fluxes tends to open a gap at finite  $T$  near the gapless-gapped boundary.

The Kitaev model is composed of  $S = 1/2$  spins defined on a honeycomb lattice, whose Hamiltonian is given by

$$\mathcal{H} = -J_x \sum_{\langle jk \rangle_x} \sigma_j^x \sigma_k^x - J_y \sum_{\langle jk \rangle_y} \sigma_j^y \sigma_k^y - J_z \sum_{\langle jk \rangle_z} \sigma_j^z \sigma_k^z, \quad (1)$$

where  $\sigma_j^l$  is the  $l (= x, y, z)$  component of the Pauli matrix representing an  $S = 1/2$  spin at site  $j$ . Corresponding to three inequivalent bonds on the honeycomb lattice, named  $x$ ,  $y$ , and  $z$  bonds, the sum over  $\langle jk \rangle_l$  is taken over the nearest neighbor (NN) sites on the  $l$  bonds. The ground state of the model was exactly shown to be gapped and gapless QSLs depending on the exchange parameters,  $J_x$ ,  $J_y$ , and  $J_z$  [5] [see the inset of Fig. 1(p)]. The spin correlations are extremely short-ranged, i.e., nonzero only for the NN pairs [16]. The model does not exhibit any phase transition at finite  $T$  although a three-dimensional variant does [14].

An exact solution of the Kitaev model is formulated by the Jordan-Wigner transformation along the chains consisting of the  $x$  and  $y$  bonds [7–9]. The fermions introduced by the transformation can be represented by two Majorana fermions  $c_j$  and  $\bar{c}_j$  at each site  $j$ . Using these Majorana fermions, the Kitaev model is rewritten as

$$\mathcal{H} = iJ_x \sum_{\langle jk \rangle_x} c_j c_k - iJ_y \sum_{\langle jk \rangle_y} c_j c_k - iJ_z \sum_{\langle jk \rangle_z} \eta_r c_j c_k, \quad (2)$$

where  $j < k$  is satisfied on the NN bonds. The operator  $\eta_r = i\bar{c}_j \bar{c}_k$  is defined on each  $z$  bond ( $r$  is the bond index) and satisfies  $\eta_r^2 = 1$ . Moreover, this is regarded as a classical variable taking  $\pm 1$  because of  $[\mathcal{H}, \eta_r] = 0$  for all  $r$ .

By using this formulation, the partition function  $Z$  of the Kitaev model is given by

$$Z = \text{Tr}_{\{\eta_r\}} \text{Tr}_{\{c_i\}} e^{-\beta \mathcal{H}} = \sum_{\{\eta_r\}=\pm 1} e^{-\beta F_f(\{\eta_r\})}, \quad (3)$$

where  $\text{Tr}_{\{\eta_r\}}$  and  $\text{Tr}_{\{c_i\}}$  are the traces for localized and itinerant Majorana fermions, respectively;  $\beta = 1/T$  is the inverse temperature (we set the Boltzmann constant  $k_B = 1$ ). Here,  $F_f(\{\eta_r\})$  is the free energy of the Majorana fermion system for a fixed configuration  $\{\eta_r\}$ , which is easily calculated by the exact diagonalization. We perform the Markov chain Monte Carlo simulation for sampling the configurations of  $\{\eta_r\}$  so as to reproduce the thermal distribution of  $e^{-\beta F_f(\{\eta_r\})}$  [14]. In the present calculations, we performed the MC simulation hybridized with the parallel tempering technique with 16 replicas [17] and spent the 10,000 MC steps for thermalization and 40,000 MC steps for measurement in up to an  $L = 12$  cluster, which contains  $N = 2 \times L^2 = 288$  sites.

Figures 1(a)-1(d) show the specific heat  $C_v$  as a function of  $T$  for several values of the anisotropy parameter  $\alpha$ ; here we define  $J_x = J_y = \alpha/3$  and  $J_z = 1 - 2\alpha/3$  so that  $J_x + J_y + J_z = 1$ . For all cases, the specific heat exhibits

two peaks; both are almost system-size independent, indicating two crossovers. We hereafter term the low- and high- $T$  crossover temperatures as  $T_L$  and  $T_H$ , respectively. The entropy per site,  $S$ , which is calculated by  $\ln 2 - \int_T^{10} dT' C_v/T'$  is shown in Figs. 1(e)-1(h). The entropy rapidly decreases with decreasing  $T$  in the vicinity of  $T_L$  and  $T_H$  corresponding to the two peaks of the specific heat. A half of the entropy is released successively in each crossover; consequently, the entropy becomes  $\sim \frac{1}{2} \ln 2$  per site in the region between  $T_L$  and  $T_H$ . The plateau-like behavior of the entropy in this region becomes clearer for smaller  $\alpha$ , i.e., larger anisotropy of the exchange constants.

Let us discuss the origins and consequences of the two crossovers. First, we focus on the crossover at  $T_H$ . The itinerant Majorana fermions  $c_i$  form a band whose width is  $W_B = 2(J_x + J_y + J_z) - \Delta = 2 - \Delta$ , where  $\Delta$  is the excitation gap in the gapped phase. Suppose that the system is in the gapless region and the density of states (DOS) is constant  $\sim 1/W_B$ , the specific heat originating from the itinerant Majorana fermions takes maximum at  $T \sim 0.511$ . This value well coincides with  $T_H$  in a wide region of  $\alpha$  including the gapped region. The result clearly indicates that the high- $T$  crossover originates in the itinerant Majorana fermions.

We find that the crossover at  $T_H$  is closely related with the development of short-range spin correlations. In the Kitaev model, the spin correlation  $\langle \sigma_j^l \sigma_k^l \rangle$  is nonzero only for the NN  $\langle jk \rangle_l$  bond [16]. Thus, we measure the equal-time spin correlation by  $S^l = \frac{2}{N} \sum_{\langle jk \rangle_l} \langle \sigma_j^l \sigma_k^l \rangle$ , which is given by each term in Eq. (2) in terms of Majorana fermions. The  $T$  dependences of  $S^l$  are presented in Figs. 1(i)-1(l) for the same set of  $\alpha$  as in Figs. 1(a)-1(h). In the high- $T$  limit,  $S_{jk}^l$  is given by the high- $T$  expansion as  $\text{Tr}[\sigma_j^l \sigma_k^l e^{-\beta \mathcal{H}}] / \text{Tr} e^{-\beta \mathcal{H}} \sim -\beta \text{Tr}[\sigma_j^l \sigma_k^l \mathcal{H}] = \beta J_l$ . Our QMC data obey this Curie behavior, indicated by the dashed-dotted curves in Figs. 1(i)-1(l). In the crossover region near  $T_H$ , however, the spin correlations show deviations from the Curie behavior, and quickly saturate to the values that are analytically obtained for the ground state (horizontal dashed lines in the figures). Hence, the high- $T$  crossover by the itinerant Majorana fermions corresponds to physically important behavior in this quantum spin system: the growth of the short-range spin correlations. We note that the spin correlations also show slight changes in the low- $T$  crossover at  $T_L$ . This behavior is discussed later.

Next, we discuss what occurs in the low- $T$  crossover. The entropy release near  $T_L$  originates from the localized Majorana fermions  $\bar{c}_j$  or  $\eta_r$ . This is confirmed by calculating the  $T$  dependence of the flux composed of the localized Majorana fermions  $\bar{c}_j$  as  $W_p = \prod_{r \in p} \eta_r$ , where  $p$  denotes the hexagonal plaquette in the honeycomb lattice. The thermal average of the flux density  $W = \frac{2}{N} \sum_p \langle W_p \rangle$  is presented in Figs. 1(e)-1(h). The results show that  $W$  rapidly decreases from 1 with increasing  $T$  in the vicinity of  $T_L$ . Hence, the crossover at  $T_L$  is due to the thermal fluctuation of fluxes.

This is further confirmed by considering the toric code limit corresponding to  $J_x, J_y \ll J_z$  ( $\alpha \ll 1$ ). In this limit,

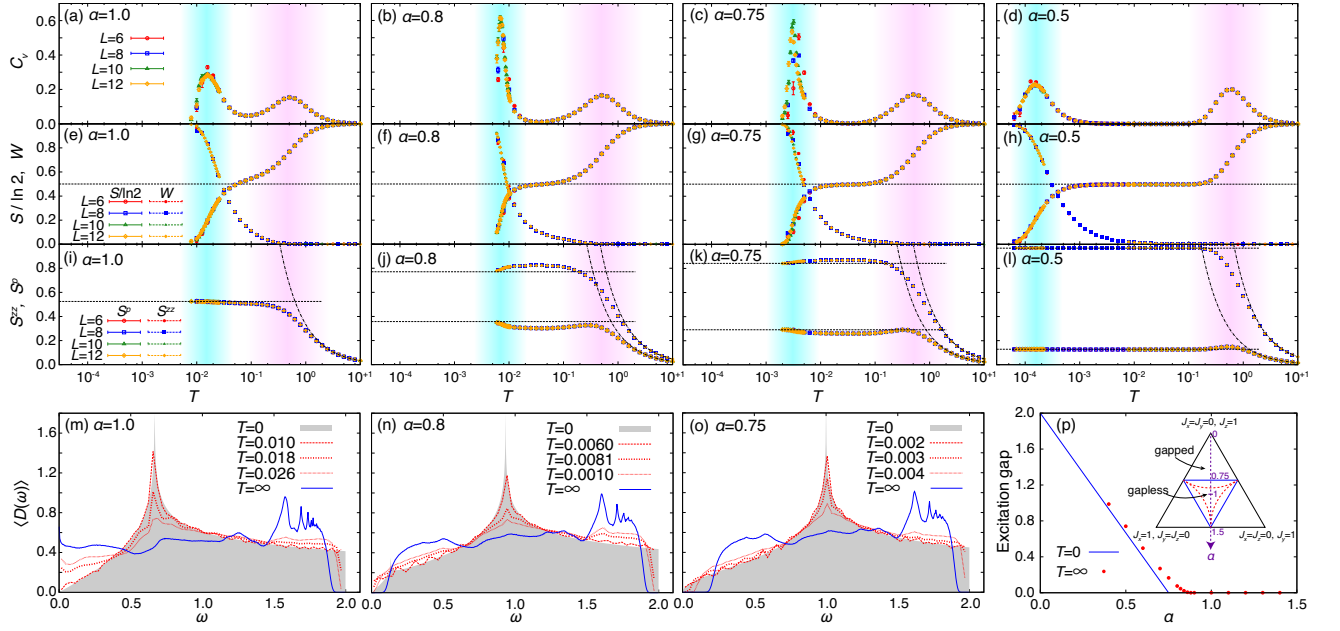


FIG. 1: (color online). (a)-(d)  $T$  dependences of the specific heat at (a)  $\alpha = 1.0$ , (b)  $\alpha = 0.8$ , (c)  $\alpha = 0.75$ , and (d)  $\alpha = 0.5$  in the several clusters with  $2 \times L^2$  spins. Here, we define the anisotropy parameter  $\alpha$  by taking  $J_x = J_y = \alpha/3$  and  $J_z = 1 - 2\alpha/3$ . (e)-(h)  $T$  dependences of the entropy per site,  $S$ , and the thermal average of the density of the flux  $W_p$ ,  $W$ . (i)-(l)  $T$  dependences of the equal-time spin correlations,  $S^{ll}$ ;  $S^p = (S^{xx} + S^{yy})/2$ . The horizontal dashed lines represent the values at  $T = 0$  which are calculated analytically [16], and the dashed-dotted curves represent the high- $T$  Curie behaviors  $S^{ll} \sim J_l/T$ . (m)-(o) The DOS of Majorana fermions at (m)  $\alpha = 1.0$ , (n)  $\alpha = 0.8$ , and (o)  $\alpha = 0.75$ . Except the results at  $T = 0$  and  $T = \infty$ , the DOS are calculated by QMC for the  $10 \times 10$  superlattice of the  $L = 12$  cluster. (p) The excitation gap for the Majorana fermions at  $T = 0$  (blue solid line) and  $T = \infty$  (red symbols) as a function of  $\alpha$ . The inset indicates the gapped-gapless boundaries on the plane of  $J_x + J_y + J_z = 1$ . The blue solid lines represent the phase boundaries in the ground state, while the red dashed lines represent the boundaries obtained from the DOS at  $T = \infty$ . See the text for details.

the Kitaev model is reduced to the effective model  $\mathcal{H}_{\text{eff}} = -J_{\text{eff}} \sum_p W_p$ , where  $J_{\text{eff}} = J_x^2 J_y^2 / (16 J_z^3)$  [5]. Since this effective model describes free Ising spins in the magnetic field  $J_{\text{eff}}$ , the specific heat is of Schottky-type, which takes a maximum at  $\tilde{T}_L / J_{\text{eff}} \sim 0.833$ . This asymptotic behavior well explains  $T_L$  in the small  $\alpha$  region (see also Fig. 2).

The crossover behavior is summarized in Fig. 2. As mentioned above, the high- $T$  crossover temperature  $T_H$  is almost constant  $\sim 0.511$  (the dashed-dotted line) independent of  $\alpha$ . On the other hand, the low- $T$  crossover temperature  $T_L$  strongly depends on  $\alpha$ . The behavior in the small  $\alpha$  region well agrees with the asymptotic form obtained in the toric code limit (the dashed curve). Thus, the phase diagram is divided into three regions: the high- $T$  paramagnetic region for  $T \gtrsim T_H$ , the intermediate- $T$  region for  $T_L \lesssim T \lesssim T_H$  where quantum spins develop short-range correlations while the fluxes remain disordered, and the low- $T$  region for  $T \lesssim T_L$  where fluxes are aligned uniformly.

Since the  $Z_2$  variables  $\eta_r$  couple with the itinerant Majorana fermions, we expect that the enhanced fluctuations of fluxes near  $T_L$  affect the nature of itinerant Majorana fermions considerably. In order to elucidate such behavior, we calculate the DOS of itinerant Majorana fermions. The DOS with a given configuration of  $\eta_r$  is calculated by  $D(\omega, \{\eta_r\}) =$

$\sum_n \delta(\omega - E_n(\{\eta_r\}))$ , where  $E_n$  is the one-particle energy of the fermion  $f_n$  which is introduced so as to diagonalize the Hamiltonian as  $\mathcal{H}(\{\eta_r\}) = \sum_n E_n(\{\eta_r\}) (f_n^\dagger f_n - \frac{1}{2})$ . The thermal averages of the DOS,  $\langle D(\omega) \rangle$ , are calculated for  $\{\eta_r\}$  generated in the QMC simulation. Note that  $\langle D(\omega) \rangle$  do not contain the  $T$  dependence of the Fermi distribution function; we only take into account the effect of thermal fluctuations of  $\eta_r$ . The calculations were done for the  $10 \times 10$  supercell, where the  $L = 12$  cluster obtained by the MC simulation is regarded as a unit cell. The calculations at  $T = 0$  ( $T = \infty$ ) are performed for a  $L = 6,000$  ( $L = 60$ ) cluster. In the calculation at  $T = \infty$ , we take a simple average over 10,000 random configurations of  $\{\eta_r\}$ .

Figure 1(m) shows the DOS of the itinerant Majorana fermion  $c_j$  for the isotropic case  $J_x = J_y = J_z$ . The QMC data are shown near  $T_L$ , together with the results at  $T = 0$  and  $T = \infty$ . In this gapless QSL region, at  $T = 0$ , the DOS shows semimetallic behavior  $D(\omega) \propto \omega$  for small  $\omega$ , reflecting the Dirac dispersion. While increasing  $T$  above  $T_L$ , however, the semimetallic dip of DOS is filled rapidly, leading to “metallic” behavior,  $\langle D(\omega = 0) \rangle \neq 0$ . The result clearly indicates that the thermal fluctuations of fluxes near  $T_L$  significantly affect the low-energy spectrum of itinerant Majorana fermions.

This significant change in the DOS results in a peculiar  $T$

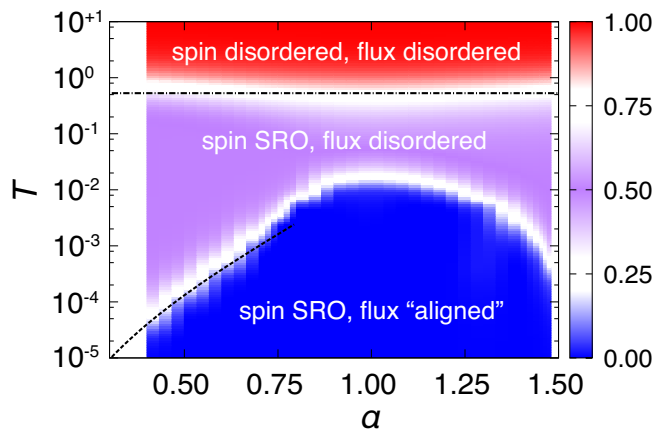


FIG. 2: (color online). Contour map of the entropy per site,  $S/\ln 2$ , on a plane of  $T$  and  $\alpha$ . The dashed line represents crossover temperature obtained by the perturbation theory in the limit of  $J_z \gg J_x, J_y$  ( $\alpha \ll 1$ ). The dashed-dotted line represents the crossover temperature obtained by assuming the constant DOS. SRO stands for a short-range order.

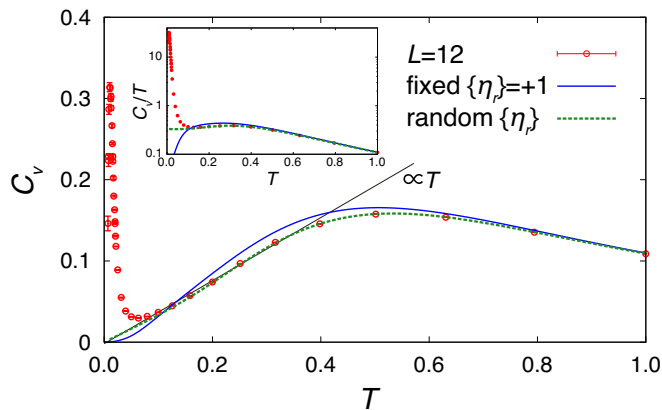


FIG. 3: (color online).  $T$  dependence of the specific heat  $C_v$  at  $\alpha = 1.2$  in the  $L = 12$  cluster. For comparison, the results calculated by fixing all  $\eta_r$  to  $+1$  and by assuming random  $\{\eta_r\}$  are shown as the solid and dashed curves, respectively. The semilog plot of  $C_v/T$  is also shown in the inset.

dependence of the specific heat  $C_v$ . In the gapless QSL region, the low- $T$  specific heat is expected to be proportional to  $T^2$  because of the Dirac semimetallic dispersion for aligned fluxes ( $\eta_r = +1$  for all  $r$ ). However,  $C_v$  calculated by assuming all  $\eta_r = +1$  largely deviates from our QMC data, as shown for  $\alpha = 1.2$  in Fig. 3. This indicates that the asymptotic  $T^2$  behavior will be limited only in the low  $T$  region much lower than  $T_L$ . Instead, we find that the QMC data are well explained by the result for random  $\{\eta_r\}$  in a wide range of  $T \gtrsim T_L$ . Consequently,  $C_v$  exhibits apparent  $T$ -linear behavior between  $T_L$  and  $T_H$ , originating from the “metallic” DOS caused by thermally fluctuating fluxes above  $T_L$ . Thus,

we find that the specific heat of the Kitaev model in Eq. (1) behaves like  $T$ -linear, not  $T^2$  as expected, as a consequence of the thermal fractionalization of quantum spins. Interestingly, the apparent  $T$ -linear behavior is observed in the region where the short-range spin correlations are well developed.

Whereas the  $T$ -linear behavior is observed widely in the region where the ground state is gapless, it is disturbed in the vicinity of the gapped-gapless boundary at  $\alpha = 0.75$ . Figures 1(n) and 1(o) show the DOS of the itinerant Majorana fermions at  $\alpha = 0.8$  and  $\alpha = 0.75$ , respectively. At these parameters, the system develops an energy gap with increasing  $T$  in the vicinity of  $T_L$ , in sharp contrast to the gap filling in Fig. 1(m). The results indicate that there is an intermediate region where the thermal fluctuation of  $\eta_r$  gaps out the low-energy excitation of itinerant Majorana fermions. The intermediate region is identified by calculating the magnitudes of the gaps at  $T = 0$  and  $T = \infty$ , as presented in Fig. 1(p). The schematic phase diagram determined by the DOS at  $T = \infty$  is presented in the inset. Remarkably, the gapped-gapless boundary is similar to that in the dynamical phase diagram [18], suggesting a relation between thermal and quantum fluctuations. We also note that the boundary is similar to the result for the full flux state [19]. The modification of the boundary at finite  $T$  implies that effective exchange couplings are renormalized in an anisotropic way by the thermal fluctuation of localized Majorana fermions. Indeed, the anisotropy of spin correlations is slightly enhanced near  $T_L$  while increasing  $T$ , as shown in Figs. 1(j) and 1(k).

In summary, we have investigated the thermal fractionalization of quantum spins into Majorana fermions in the Kitaev model by using the QMC simulation. We clarified that the fractionalization appears as two crossovers, both of which are physically observable in the thermodynamics. The higher- $T$  crossover is identified by the development of short-range spin correlations, which will be observed in, e.g., neutron scattering experiments. Meanwhile, the low- $T$  one induces a peculiar  $T$  linear behavior in the specific heat above the crossover temperature. We also showed that the thermal fractionalization affects the gapped-gapless phase boundary by renormalizing the spin anisotropy. The present results complete how the fractionalization of quantum spins into Majorana fermions occurs while changing temperature in the ideal case. This provides a useful reference to the experimental exploration of QSLs in, e.g., iridium oxides [20–24] and ruthenium compounds [25–28], where Kitaev-type interaction is expected.

This work is supported by Grant-in-Aid for Scientific Research, the Strategic Programs for Innovative Research (SPIRE), MEXT, and the Computational Materials Science Initiative (CMSI), Japan. Parts of the numerical calculations are performed in the supercomputing systems in ISSP, the University of Tokyo.

[1] S. Tomonaga, Prog. Theor. Phys. **5**, 544 (1950).

- [2] X. G. Wen, Phys. Rev. B **44**, 2664 (1991).
- [3] C. Castelnovo, R. Moessner, and S. L. Sondhi, Nature **451**, 42 (2008).
- [4] V. J. Emery and S. Kivelson Phys. Rev. B **46**, 10812 (1992).
- [5] A. Kitaev, Ann. Phys. **321**, 2 (2006).
- [6] G. Jackeli and G. Khaliullin, Phys. Rev. Lett. **102**, 017205 (2009).
- [7] H.-D. Chen and J. Hu, Phys. Rev. B **76**, 193101 (2007).
- [8] X.-Y. Feng, G.-M. Zhang, and T. Xiang, Phys. Rev. Lett. **98**, 087204 (2007).
- [9] H.-D. Chen, and Z. Nussinov, J. Phys. A Math. Theor. **41**, 075001 (2008).
- [10] J. Chaloupka, G. Jackeli, and G. Khaliullin, Phys. Rev. Lett. **105**, 027204 (2010).
- [11] J. Reuther, R. Thomale, and S. Trebst, Phys. Rev. B **84**, 100406 (2011).
- [12] J. Chaloupka, G. Jackeli, and G. Khaliullin, Phys. Rev. Lett. **110**, 097204 (2013).
- [13] J. Nasu, T. Kaji, K. Matsuura, M. Udagawa, and Y. Motome, Phys. Rev. B **89**, 115125 (2014).
- [14] J. Nasu, M. Udagawa, and Y. Motome, Phys. Rev. Lett. **113**, 197205 (2014).
- [15] J. Nasu, M. Udagawa, and Y. Motome, J. Phys.: Conf. Ser. **592**, 012115 (2015).
- [16] G. Baskaran, S. Mandal, and R. Shankar, Phys. Rev. Lett. **98**, 247201 (2007).
- [17] K. Hukushima and K. Nemoto, J. Phys. Soc. Jpn. **65**, 1604 (1996).
- [18] J. Knolle, D. L. Kovrizhin, J. T. Chalker, and R. Moessner, Phys. Rev. Lett. **112**, 207203 (2014).
- [19] V. Lahtinen, G. Kells, A. Carollo, T. Stitt, J. Vala, J. K. Pachos, Ann. Phys. **323**, 2286 (2008).
- [20] Y. Singh and P. Gegenwart, Phys. Rev. B **82**, 064412 (2010).
- [21] Y. Singh, S. Manni, J. Reuther, T. Berlijn, R. Thomale, W. Ku, S. Trebst, and P. Gegenwart, Phys. Rev. Lett. **108**, 127203 (2012).
- [22] S. K. Choi, R. Coldea, A. N. Kolmogorov, T. Lancaster, I. I. Mazin, S. J. Blundell, P. G. Radaelli, Y. Singh, P. Gegenwart, K. R. Choi, S.-W. Cheong, P. J. Baker, C. Stock, and J. Taylor, Phys. Rev. Lett. **108**, 127204 (2012).
- [23] R. Comin, G. Levy, B. Ludbrook, Z.-H. Zhu, C. N. Veenstra, J. A. Rosen, Y. Singh, P. Gegenwart, D. Stricker, J. N. Hancock, D. van der Marel, I. S. Elfimov, and A. Damascelli, Phys. Rev. Lett. **109**, 266406 (2012).
- [24] K. Ohgushi, J. I. Yamaura, H. Ohsumi, K. Sugimoto, S. Takeshita, A. Tokuda, H. Takagi, M. Takata, and T. H. Arima, Phys. Rev. Lett. **110**, 217212 (2013).
- [25] K. W. Plumb, J. P. Clancy, L. J. Sandilands, V. V. Shankar, Y. F. Hu, K. S. Burch, H. Y. Kee, and Y. J. Kim, Phys. Rev. B **90**, 041112 (2014).
- [26] Y. Kubota, H. Tanaka, T. Ono, Y. Narumi, and K. Kindo, Phys. Rev. B **91**, 094422 (2015).
- [27] J. A. Sears, M. Songvilay, K. W. Plumb, J. P. Clancy, Y. Qiu, and Y. Kim, arXiv:1411.4610.
- [28] M. Majumder, M. Schmidt, H. Rosner, A. A. Tsirlin, H. Yasuoka, and M. Baenitz, arXiv:1411.6515.